

# Infrared Spectrum of 4-Methoxypicolinic Acid *N*-Oxide: Computation of Asymmetric O–H Stretching Band<sup>†</sup>

Katja Balažic, Jernej Stare, and Janez Mavri\*

National Institute of Chemistry, Hajdrihova 19, 1000, Ljubljana, Slovenia

Received November 14, 2006

In this article we studied the strong intramolecularly hydrogen-bonded system 4-methoxypicolinic acid *N*-oxide. The potential energy surface  $V = V(r_{\text{OH}}, r_{\text{OO}})$  and the corresponding dipole moment function were calculated using the DFT B3LYP/6-31+G(d,p) level of approximation. The time-independent vibrational Schrödinger equation was solved using a rectangular grid basis set and shifted Gaussian basis set. The vibrational spectrum and metric parameters were also calculated. Effects of deuteration were considered. The calculated vibrational spectra were compared with the experimental spectra. The vibrational transition corresponding to asymmetric O–H stretching that occurs at about  $1400\text{ cm}^{-1}$  compares well with the experimentally assigned O–H asymmetric stretching band centered at  $1380\text{ cm}^{-1}$ . The corresponding asymmetric O–D stretching band was predicted to be at  $1154\text{ cm}^{-1}$ , while the experimental O–D band was not assigned due to its very low intensity. Several overtones and hot transitions of significant intensities were located in the vicinity of the fundamental O–H stretching frequency, effectively broadening the infrared absorption attributed to the O–H stretching mode. This is in a good agreement with the observed broad protonic absorptions found in the infrared spectra of the title compound and its analogs. We have shown that the Gaussian basis set is the method of choice for a two-dimensional vibrational problem that requires several hundreds of vibrational basis functions and when high accuracy of the eigenvalues is required or when extending the calculations to more vibrational degrees of freedom. We have also demonstrated that for a large number of basis functions the Gramm-Schmidt orthogonalization procedure outperforms symmetric and canonical orthogonalization schemes.

## 1. INTRODUCTION

Modeling of short hydrogen bonds represents a major challenge due to significant anharmonicity and quantum nature of the proton motion. Understanding the properties of short hydrogen bonds is of prime importance for biological processes. Recently, a large number of experimental and computational studies have addressed the structure and dynamics of hydrogen bonds.<sup>1–10</sup> In this article we studied vibrational properties of a strong hydrogen-bonded system, namely 4-methoxypyridine 1-oxide 2-carboxylic acid (4-methoxypicolinic acid *N*-oxide, abbreviated MPANO, Figure 1). This compound contains a very short intramolecular hydrogen bond. Several experimental methods were used for studying the nature of this hydrogen bond: the enormous chemical shift of 20.25 ppm of the H-bonded proton in dimethylsulfoxide solution by NMR<sup>11</sup> and the O–H stretching band at about  $1380\text{ cm}^{-1}$  via IR spectroscopy (solid state and solutions of various solvents).<sup>12</sup> A detailed overview of the whole family of picolinic acid *N*-oxide and related compounds is given in ref 12. The study of this series of compounds is still in progress and will be published elsewhere.

It is well-known that a potential energy surface of the O–H...O moieties in strong hydrogen bonds is highly anharmonic.<sup>13</sup> This is why the harmonic treatment is not

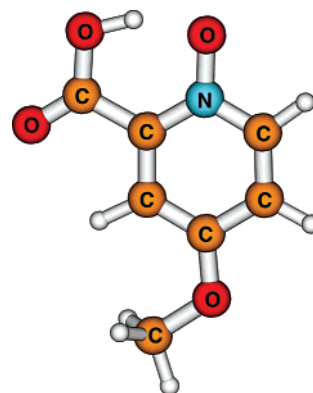


**Figure 1.** The B3LYP/6-31+G(d,p) global minimum structure of 4-methoxypicolinic acid *N*-oxide (MPANO).

sufficient for a reliable determination of vibrational frequencies. Namely, the B3LYP/6-31+G(d,p) harmonically calculated O–H stretching frequency in MPANO is  $2783\text{ cm}^{-1}$  compared to an experimental value of about  $1380\text{ cm}^{-1}$  (in chloroform solution).<sup>12</sup> It is therefore necessary to include anharmonic effects in the applied theoretical method. Worth noting is that the environmental effects also play an important role and need to be considered.<sup>14</sup> In the present work we considered only the gas-phase model.

In this article we examined the nature of the intramolecular hydrogen bond in MPANO. We constructed a two-dimensional energy surface  $V = V(r_{\text{OH}}, r_{\text{OO}})$  and a corresponding dipole moment surface. The vibrational Schrödinger equation

<sup>†</sup> Dedicated to Professor Nenad Trinajstić on the occasion of his 70th birthday.

\* Corresponding author e-mail: janez@kihp2.ki.si.

was solved, and the anharmonic frequencies and IR relative intensities of the O—H···O and O···O stretching vibrations as well as their overtones and complex transitions were calculated. The effects of deuteration were also considered. We applied a rectangular grid vibrational basis set and a shifted Gaussian basis set; for the latter various basis set orthogonalization schemes were compared.

Various frequency calculation strategies beyond the harmonic approximation are available,<sup>15–20,22</sup> and all share the problem of considerable complexity and high computational costs—namely, a large number of evaluations of the potential energy is required; this number increases exponentially with the number of considered vibrational degrees of freedom. In addition, some of these strategies such as the otherwise powerful Vibrational Self-Consistent Field (VSCF) method<sup>16,17</sup> are less appropriate for the treatment of highly anharmonic, large-amplitude vibrations associated with short hydrogen bonds. In the present work, we utilized a special version of a variational code for the numerical solving of the vibrational Schrödinger equation (SE) in internal coordinates, tuned for application to hydrogen-bonded systems.<sup>21,22</sup>

This article is organized as follows: the theoretical background for solving the time-independent vibrational Schrödinger equation is outlined in section 2; computational details are given in section 3; the results are collected and discussed in section 4; and concluding remarks are made in section 5. Details of the Gram-Schmidt orthogonalization together with the comparison of the performance of various orthogonalization routines are given in the Appendix.

## 2. THEORY

Our computational method is based on the vibrational time-independent SE for a given potential energy surface (PES), solved using the variational principle in either a rectangular grid or a Gaussian vibrational basis set representation. This method, incorporated in a program package, is described in detail by Stare and Mavri.<sup>21</sup> An update of the program package that includes kinetic coupling was performed.<sup>22</sup> While grid basis functions are local constants, the two-dimensional Gaussian basis functions have the functional form  $\phi = Ne^{-\alpha(x-a)^2}e^{-\beta(y-b)^2}$ , where  $a$  and  $b$  are coordinates of the center of the Gaussian,  $\alpha$  and  $\beta$  are the exponential constants, and  $N$  is the normalization factor.

The vibrational SE becomes a matrix equation when the variational principle is applied and has the following form:

$$\mathbf{HC} = \mathbf{SCE} \quad (1)$$

The matrix  $\mathbf{H}$  is the Hamiltonian for the given basis set, and  $\mathbf{S}$  is the overlap matrix of that basis set.  $\mathbf{C}$  is the matrix of the coefficients of the resulting wavefunctions, and  $\mathbf{E}$  is a diagonal matrix containing the energies. Equation 1 differs from the standard eigenvalue problem only in the overlap matrix  $\mathbf{S}$ . In the rectangular basis set the  $\mathbf{S}$  term is a unity matrix and diagonalization can be directly applied, while in the Gaussian basis set an orthogonalization procedure must be carried out prior to the diagonalization. Orthogonalization transforms eq 1 into the standard eigenvalue problem

$$\mathbf{H}'\mathbf{C}' = \mathbf{C}'\mathbf{E} \quad (2)$$

where the primes denote the Hamiltonian, and the coefficients are represented in an orthogonal base.  $\mathbf{H}'$  is obtained from

$\mathbf{H}$  by orthogonalization of matrix  $\mathbf{X}$  according to the equation (symmetric orthogonalization)

$$\mathbf{H}' = \mathbf{X}^\dagger \mathbf{H} \mathbf{X} \quad (3)$$

where  $\mathbf{X}^\dagger$  is the adjoint matrix (i.e., the conjugate transpose) of  $\mathbf{X}$ . The coefficient matrices in both bases are related by the equation  $\mathbf{C} = \mathbf{X}\mathbf{C}'$ .

There are various ways of obtaining  $\mathbf{X}$  from  $\mathbf{S}$ . Symmetric and *canonical* orthogonalization procedures are based on the diagonalization of  $\mathbf{S}$  and taking inverse square roots of its eigenvalues. Canonical orthogonalization is preferred over symmetric because it can eliminate nearly linearly dependent functions. An alternative to symmetric and canonical orthogonalization is the *Gram-Schmidt* algorithm (GS),<sup>23,24</sup> which we have implemented and critically examined in this article (see the Appendix for details).

Once the solution of the vibrational SE (energies and wavefunctions of the ground state and the excited states) is determined, one can derive several other quantities. Among these are the thermally averaged expectation values of the vibrational coordinates, which may be regarded as optimized metric parameters that include thermal corrections for the quantum behavior of the nuclei. The other useful quantities that can be derived are the relative IR intensities for the transitions in the O—H···O moiety, given that a dipole moment hypersurface is provided. Realistic systems, like hydrogen-bonded moieties, exhibit not only *mechanical anharmonicity* (i.e., deviation of the PES from the parabolic shape) but also *electrical anharmonicity*, meaning that the dipole moment is no longer a linear function of the coordinates. The latter affects the intensities but not the position of the peaks in the vibrational spectrum. Both anharmonicities affect the selection rules for transitions between the vibrational levels; in general, transitions between all the levels are possible beyond the double harmonic approximation.

In the present article the PES is represented by the O—H and O···O stretching internal coordinates, that is, by the corresponding interatomic distances. We calculated the PES  $V = V(r_{\text{OH}}, r_{\text{OO}})$  and the corresponding dipole moment surface. Such a choice of vibrational coordinates is well established<sup>21,25–27</sup> and is reasonable because of strong potential energy coupling between the high- and low-frequency modes in hydrogen bonds. Inclusion of other vibrational degrees of freedom such as the C—O—H bond angle or the N—O bond distance, etc., would represent a desirable improvement of the calculation (as is the case of a study performed by one of the authors (J.S.) that suggests notable coupling between the O—H stretching and C—O—H bending coordinates in a closely related hydrogen-bonded system<sup>22</sup>); however, the present computer resources prevented us from using more than two degrees of freedom.

## 3. COMPUTATIONAL DETAILS

All electron structure calculations were performed by the Gaussian 03 program package.<sup>28</sup> One of the most crucial parts of the applied program is the proper fitting of certain analytical functional forms to the original points of the PES, provided by *ab initio* or Density Functional Theory (DFT) calculations. In this article, we consider the two-dimensional PES; the chosen coordinates were the O—H

**Table 1.** Fitted Parameters of the Potential Energy Surface in the Functional Form of  $V(x,y) = \text{HC} + \sum_{i=1}^{15} A_i e^{-\alpha_i^2(x-x_i^0)^2} e^{-\beta_i^2(y-y_i^0)^2}$ 

<i>i</i>	location of the center		exponential factors		coefficients $A_i$
	$x_i^0$ (Å)	$y_i^0$ (Å)	$\alpha_i$ (Å <sup>-1</sup> )	$\beta_i$ (Å <sup>-1</sup> )	
1	-12.020	5.054	58.978	22.946	-79.079
2	-0.561	11.213	-66.080	-26.616	-66.898
3	15.532	-18.011	-0.934	0.236	-13.799
4	1.065	2.573	2.623	5.330	-4.224
5	-2.324	2.418	0.700	6.486	-304.223
6	0.921	2.579	1.449	1.361	-87.359
7	-1.358	4.645	0.035	0.558	-51.385
8	1.390	2.364	-4.629	4.842	-7.050
9	1.445	2.028	0.766	3.894	-43.298
10	-14.082	4.655	0.030	-0.843	-92.606
11	1.699	2.291	1.031	-3.922	-38.654
12	0.949	3.776	2.248	0.633	-54.161
13	2.095	2.786	1.603	-2.129	-108.281
14	1.600	2.554	3.207	3.832	-28.222
15	0.797	14.446	13.061	-0.062	32.878

<sup>a</sup> Where HC is 150 kcal/mol, for the hydrogen bond in 4-methoxypicolinic acid *N*-oxide. The Gaussians are suspended from a 'hard core ceiling' to ensure correct asymptotic behavior of the potential energy surface. Note that  $x$  and  $y$  represent the O–H and the O···O stretching coordinates, respectively.

**Table 2.** Matrix of the Fitted Polynomial Coefficients  $a_{ij}$  of the Dipole Moment Surface for 4-Methoxypicolinic Acid *N*-Oxide in the Functional Form  $\mu(x,y) = \sum_{i=0}^5 \sum_{j=0}^5 a_{ij} x^i y^j$ 

<i>i/j</i>	0	1	2	3	4	5
0	28.481	-20.213	-32.179	52.212	-23.672	3.306
1	23.943	8.641	-25.566	-24.970	29.159	-5.654
2	-5.214	32.502	25.450	-29.682	-6.792	3.337
3	-54.200	14.362	40.989	-7.233	5.039	-1.641
4	-51.170	-2.127	12.843	-13.909	3.073	0.022
5	40.778	2.491	-34.012	22.046	-5.389	0.444

<sup>a</sup> The units are given in Debye · Å<sup>-(i+j)</sup>. Note that  $x$  and  $y$  represent the O–H and the O···O stretching coordinates, respectively.

**Table 3.** Frequencies (in cm<sup>-1</sup>) of the Fundamental O–H(D) and O···O Vibrational Transitions in 4-Methoxypicolinic Acid *N*-Oxide (MPANO), for Both the Undeuterated and Deuterated Compounds<sup>a</sup>

	harmonic calculation		1D PES		2D PES		expt <sup>b</sup> $\nu_{\text{OH(D)}}$
	$\nu_{\text{OO}}$	$\nu_{\text{OH(D)}}$	$\nu_{\text{OO}}$	$\nu_{\text{OH(D)}}$	$\nu_{\text{OO}}$	$\nu_{\text{OH(D)}}$	
H	297	2783	295	1699	297	1407	~ 1380
D	293	2042	272	1490	274	1154	not assigned

<sup>a</sup> Calculated in the harmonic approximation using the Gaussian at the B3LYP/6-31+G(d,p) level of theory ('harmonic calculation' columns) and from one-dimensional and two-dimensional (O–H, O···O) potential energy surfaces by solving the vibrational SE ('1D PES' and '2D PES' columns). The experimental value of the O–H stretching band centroid of MPANO in chloroform solution is also listed. Note that the O···O stretching band was not experimentally assigned and that no O–D stretching band could be detected in the deuterated MPANO. <sup>b</sup> See ref 12.

( $\equiv x$ ) and O···O ( $\equiv y$ ) distances. The PES was provided by pointwise calculations at the B3LYP/6-31+G(d,p) level of theory, which proved to yield convergent optimized geometries and harmonic frequencies with respect to the level of theory. For instance, the B3LYP/6-311++G(2d,2p) level gave the O···O distance of 2.487 Å, the O–H distance of 1.017 Å, and the O–H stretching harmonic frequency of 2801 cm<sup>-1</sup>, which is only marginally different from the actually used basis set (see Tables 4 and 3). The MP2/6-31+G(d,p) results gave the values of 2.504 Å, 1.014 Å, and

**Table 4.** O–H and O···O Distances in 4-Methoxypicolinic Acid *N*-Oxide<sup>a</sup>

method/model	$\langle r_{\text{OH}} \rangle$	$\langle r_{\text{OO}} \rangle$
B3LYP/6-31+G(d,p)	1.022	2.489
quantum averaged (H); ground state	1.089	2.454
neutron diffraction <sup>b</sup>	1.172	2.405
quantum averaged (H); 298 K	1.086	2.461
quantum averaged (D); 298 K	1.062	2.473

<sup>a</sup> Calculated by plain B3LYP/6-31+G(d,p) geometry optimization and by quantum averaging from 2D vibrational wavefunctions of ground and excited states at 298 K. Experimental distances for the undeuterated compound, obtained by neutron diffraction at 20 K, are also listed (Th. Steiner, private communication). <sup>b</sup> Th. Steiner, to be published.

2931 cm<sup>-1</sup>, respectively, which is also very close to the B3LYP results. Given that the MP2 calculations require by far larger computing resources (about 10 times longer CPU time and about 100 times larger disk space relative to the corresponding B3LYP calculation) for no significant change in the results, we decided to proceed with the B3LYP/6-31+G(d,p) approximation.

At each point of the scan the O–H and O···O distances were kept constant, while the residual degrees of freedom were optimized. We considered the O···O distance range of 2.0–3.2 Å and the O–H distance range of 0.8–2.3 Å. A total number of 154 points were calculated in this way. Next, a set of 15 displaced Gaussian functions, suspended from a so-called 'hard core ceiling' (HC) of 150 kcal/mol above the global minimum of the PES, were fitted to the original points. The functional form of the PES can thus be written as

$$V(x,y) = \text{HC} + \sum_{i=1}^{15} A_i e^{-\alpha_i^2(x-x_i^0)^2} e^{-\beta_i^2(y-y_i^0)^2} \quad (4)$$

where HC denotes the hard core potential of 150 kcal/mol,  $A_i$  are the coefficients of the linear combination,  $x_i^0$  and  $y_i^0$  are the location of the center, and  $\alpha_i$  and  $\beta_i$  the exponential factors of the  $i$ th Gaussian. The fitting included the coefficients of the linear combination of the Gaussians (linear parameters) as well as their centers and exponential factors (nonlinear parameters). Since the fitting error should be small in the lower region of the PES, the points were weighted reciprocally to their energies. The fitted coefficients of the PES are given in Table 1. The overall fitting error was 0.136 kcal/mol per point, while in the lowest region of the PES (less than 10 kcal/mol above the minimum) the error was 0.059 kcal/mol per point. The contour plot of the PES is shown in Figure 2. The dipole moment surface (not shown), calculated simultaneously with the PES, was represented by a 2D polynomial of the fifth degree (with all possible cross terms included), fitted to the calculated points and expressed as

$$\mu(x,y) = \sum_{i=0}^5 \sum_{j=0}^5 a_{ij} x^i y^j \quad (5)$$

Fitting of the PES and the dipole moment function was performed numerically using a quasi Newton method. For the dipole moment surface there were 36 polynomial coefficients  $\{a_{ij}\}$  to be fitted; they are listed in Table 2.



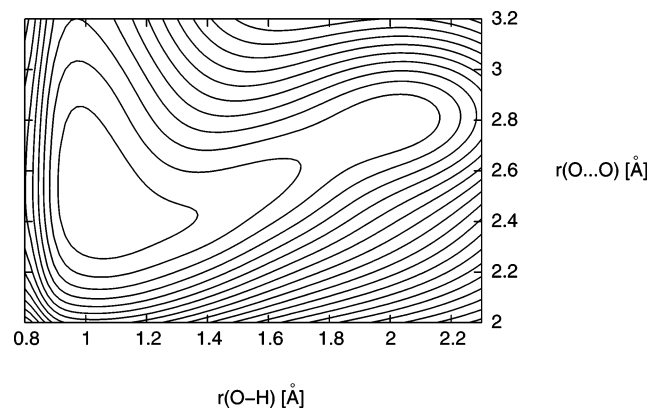


**Figure 2.** Contour plot of the potential energy surface of 4-methoxypicolinic acid *N*-oxide. The innermost contour represents the energy value of 5 kcal/mol; each successive outer contour represents a 5 kcal/mol increase in energy.

It was found that the required vibrational basis set range was from 0.70 to 2.30 Å for the  $x$  (O–H stretching) and from 2.00 to 3.40 Å for the  $y$  (O $\cdots$ O stretching) coordinate. Both the grid basis functions and also the Gaussians were placed on a rectangular grid within the above ranges, hence the total number of basis functions is equal to the product of the number of functions in both directions. Reduced masses along the  $r_{\text{OH}}$  and  $r_{\text{OO}}$  internal coordinates were evaluated according to the Wilson  $G$ -matrix formalism<sup>29</sup> (application of the  $G$ -matrix formalism to hydrogen-bonded systems is also available<sup>22</sup>). Reduced masses as reflected in the diagonal  $G$ -matrix elements were found to be constants with  $\mu_x = 0.98$  and  $\mu_y = 10.51$ , respectively. The kinetic coupling term (the off-diagonal element) was found to be negligible and was left out from our calculations.

Fitting of the PES and of the dipole moment surface as well as the solving of the SE was performed on dual CPU PC/Linux workstations. All graphical material in this article was prepared with Molden, Gnuplot, and XFig utilities.

#### 4. RESULTS

**2D PES and the Expectation Values.** Table 4 lists the values of the O–H and O $\cdots$ O distances obtained by plain geometry optimization and by thermal averaging of expectation values for the first 15 vibrational levels. It is evident that the gas-phase model yields a too large O $\cdots$ O distance relative to the solid-state experimental value. While it has been proved earlier for related systems that inclusion of periodicity improves agreement with the experiment,<sup>14,30</sup> we demonstrate in this article that inclusion of the quantum nature of the nuclei into calculations is an additional source of the O $\cdots$ O distance shrinking. In addition, the O–H distance is elongated on the inclusion of nuclear quantum effects, giving rise to improved agreement with the experiment. Comparison of the geometric parameters presented in this article to ones calculated earlier for members of the picolinic acid *N*-oxide family in various types of environments<sup>12,14,21</sup> demonstrates that the O $\cdots$ O distance shrinks in a polar environment and by quantization of the protonic vibrational modes.

Deuteration of the O–H $\cdots$ O moiety shrinks the O–H distance and elongates the O $\cdots$ O distance by 0.024 and 0.012 Å, respectively (Table 4). The shrinking of the O–D distance relative to the O–H can be explained by the fact that the

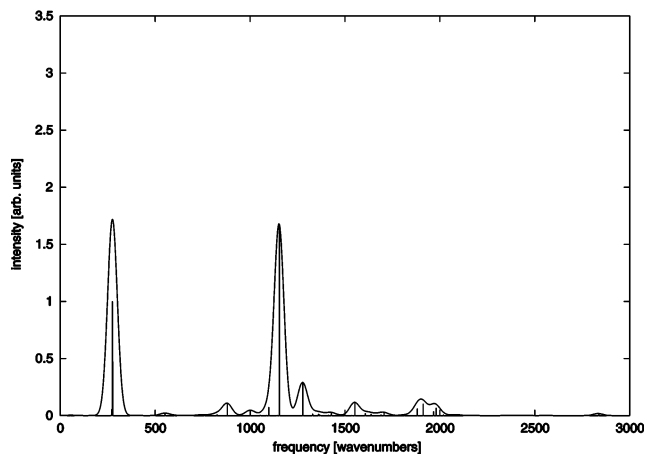
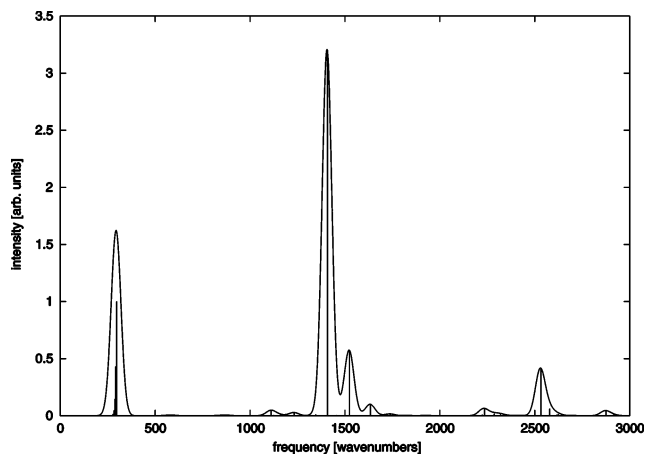


**Figure 3.** Calculated IR spectrum of undeuterated (top) and deuterated (bottom) 4-methoxypicolinic acid *N*-oxide. The bands are plotted as delta functions and overlaid by corresponding Gaussian functions with a constant half-width of 20 cm<sup>−1</sup>.

deuteron wavefunction is more localized, giving rise to a smaller expectation value of the bond distance. This is accompanied by the increase in the O $\cdots$ O distance, which is an effect common to all hydrogen bonds (i.e., the closer the hydrogen to the center of the hydrogen bond, the shorter the donor–acceptor distance). This is a secondary isotope effect referred to as the Ubbelohde effect,<sup>42</sup> its magnitude being similar to that found in closely related systems.<sup>21</sup>

**Anharmonic vs Harmonic Frequencies.** Table 3 shows the frequencies of the fundamental O–H and O $\cdots$ O stretching transitions for MPANO, calculated in the harmonic approximation as well as from the one- and two-dimensional anharmonic PES. The effects of deuteration are considered. It is evident that plain harmonic treatment fails to accurately predict the frequency of the O–H stretching band. The two-dimensional anharmonic treatment of the proton motion yields a notably lower (and thus closer to the experimentally observed) O–H stretching frequency than the one-dimensional treatment, since the former properly includes the coupling of the O $\cdots$ O stretching mode to the O–H stretching mode.

Calculated vibrational spectra of the O–H $\cdots$ O moiety for both undeuterated and deuterated MPANO are displayed in Figure 3, while their most significant components (transition frequencies and intensities) are listed in Table 5. Assignment of the transitions was performed by visualization of the corresponding vibrational eigenfunctions. From the calculated

**Table 5.** Calculated Transition Frequencies and Intensities of 4-Methoxypicolinic Acid *N*-Oxide Acquired from the Two-Dimensional Anharmonic Potential  $V = V(r_{\text{OH}}, r_{\text{OO}})$ , for Both Undeuterated and Deuterated Species<sup>a</sup>

transition $mn \rightarrow m'n'$	frequency ( $\text{cm}^{-1}$ )	relative intensity
Undeuterated Species (H)		
00 $\rightarrow$ 01	297	1
00 $\rightarrow$ 02	589	$3.7 \times 10^{-3}$
00 $\rightarrow$ 03	877	$4.8 \times 10^{-3}$
00 $\rightarrow$ 10	1407	3.2
00 $\rightarrow$ 11	1821	$2.4 \times 10^{-4}$
00 $\rightarrow$ 20	2532	0.41
01 $\rightarrow$ 02	292	0.43
01 $\rightarrow$ 10	1110	0.04
01 $\rightarrow$ 11	1524	0.57
01 $\rightarrow$ 20	2235	0.05
02 $\rightarrow$ 03	288	0.15
02 $\rightarrow$ 11	1232	0.03
02 $\rightarrow$ 12	1634	0.10
03 $\rightarrow$ 04	283	0.05
Deuterated Species (D)		
00 $\rightarrow$ 01	274	1
00 $\rightarrow$ 02	551	0.01
00 $\rightarrow$ 03	828	$6.6 \times 10^{-4}$
00 $\rightarrow$ 10	1154	1.7
00 $\rightarrow$ 11	1553	0.11
00 $\rightarrow$ 20	1981	0.07
01 $\rightarrow$ 02	277	0.47
01 $\rightarrow$ 03	553	$5.9 \times 10^{-3}$
01 $\rightarrow$ 10	880	0.11
01 $\rightarrow$ 11	1278	0.29
01 $\rightarrow$ 20	1706	0.02
02 $\rightarrow$ 03	276	0.17
02 $\rightarrow$ 11	1001	0.05
02 $\rightarrow$ 12	1361	0.01
03 $\rightarrow$ 04	271	0.06

<sup>a</sup> The transitions are labeled as  $mn \rightarrow m'n'$ , where  $m$  and  $m'$  refer to the initial and final quantum numbers along the O–H coordinate, while  $n$  and  $n'$  correspond to the initial and final quantum numbers along the O $\cdots$ O coordinate. All intensities of each isotopomer are given relative to the fundamental O $\cdots$ O stretching excitation. All hot transitions are assumed for the equilibrium state at  $T = 298$  K.

spectra one can see that the O $\cdots$ O stretching mode (00  $\rightarrow$  01) is very close to harmonicity, since its hot transitions (01  $\rightarrow$  02, 02  $\rightarrow$  03, etc.) have almost the same frequency as the fundamental band. On the other hand, the O–H stretching mode is strongly anharmonic, since its overtone (00  $\rightarrow$  20) is much less than twice the fundamental O–H excitation (00  $\rightarrow$  01). This is true for both the undeuterated and deuterated species. Moreover, as can be seen from the large O–H frequency red shift when passing from the one- to the two-dimensional potential (see Table 3), the O $\cdots$ O stretching mode is significantly coupled to the O–H motion. The portion of the spectrum that can be assigned to the O–H transitions is smeared over a large area, suggesting a broadening of the O–H band in the experimental spectrum, mainly due to the coupling with the O $\cdots$ O stretching mode; as such it is in accord with the Maréchal-Witkowski theory.<sup>31–34</sup> Note that the band contour in the calculated spectrum is obtained by assuming a standard halfwidth of  $20 \text{ cm}^{-1}$  for all the calculated transitions. This approach is not rigorous and is used for qualitative comparison. Other explanations for this broadening are the couplings of the O–H stretching to the other modes, including the solvent and dynamic effects. In order to properly take into account the latter effect one would need quantum dynamical treatment with proper inclusion of the environment.<sup>35–37</sup>

The present contribution is related to the previously published work.<sup>12,14,21,38–41</sup> The one-dimensional anharmonic vibrational O–H stretching frequency of MPANO, calculated to  $1699 \text{ cm}^{-1}$ , is notably lower than the value of  $2129 \text{ cm}^{-1}$  obtained in the same way for an unsubstituted analog (picolinic acid *N*-oxide, PANO). This indicates that the hydrogen bonding of MPANO is stronger than that of PANO, a fact that is reflected in the infrared and NMR experimental findings.<sup>11,12</sup> Del Bene and co-workers found a proton stretching frequency red shift in the HBr–NH<sub>3</sub> complex due to anharmonicity to be of the order of about  $1000 \text{ cm}^{-1}$ ,<sup>38</sup> and our findings regarding the O–H stretching red shift in MPANO are in a qualitative accord with this. Eventually, the red shift observed in this work is even larger (about  $1400 \text{ cm}^{-1}$ ), probably due to the very short O $\cdots$ O distance accompanied with large anharmonicity. In contrast to the hydrogenmaleate ion<sup>41</sup> where there is very little stretching frequency shift upon deuteration, we have found the H/D isotope ratio of the O–H stretching frequencies in MPANO to be more significant. This can be explained by a different shape of the PES as well as by constraints and artifacts of the two-dimensional approximation employed in this study.

**Intensities of the Anharmonic Transitions.** Relative intensities of the transitions, acquired from the two-dimensional PES of MPANO are shown in Table 5. The O–H stretching fundamental band appears to be of the highest intensity in MPANO, regardless of the isotopic composition. Apart from the fundamental O $\cdots$ O and O–H excitations, both the O $\cdots$ O and O–H overtones as well as the hot transitions that start from the first-excited O $\cdots$ O mode contribute significantly to the infrared spectrum of the O–H $\cdots$ O moiety of MPANO. The main difference between deuterated and undeuterated species is in that the O–H stretching overtone (00  $\rightarrow$  20 transition) has a much higher intensity in the undeuterated MPANO, while the spectrum of the deuterated species features a more pronounced complex transition resulting in simultaneous excitation of both the O $\cdots$ O and the O–D modes (00  $\rightarrow$  11 transition).

In undeuterated and deuterated MPANO the intensity ratio of the O–H and O $\cdots$ O fundamental transitions assumes values of 3.2 and 1.7, respectively. In the harmonic approximation, these ratios are larger by about an order of magnitude, namely 41 and 18. It is not clear what the significance of this difference is, but since there is no way of verifying this ratio experimentally due to the complexity of the O–H stretching absorption, we have not pursued further analysis of this aspect. However, it is worth noting that the relative O–H stretching intensity is reduced by about two on deuteration in both the harmonic and the 2D PES anharmonic calculations. This fairly agrees with the fact that the O–D band is relatively weak and probably overlapped with neighboring ring modes so that it could not be assigned in the spectrum.<sup>12</sup> At this point comparison with other hydrogen-bonded systems can be made. Computational work of Bouteiller and Latajka<sup>26</sup> on the acetone–HF intermolecular complex yields comparable, yet slightly different relative intensities of the combined protonic/slow mode stretching overtones with respect to the O $\cdots$ F stretching fundamental. In both the acetone–HF complex and MPANO the relative intensity of the 00  $\rightarrow$  11 overtone is quite low, being of the order of 2% in the acetone–HF complex and about 2 orders

of magnitude smaller in MPANO; some similarity between results of the present work and that of Bouteiller and Latajka can also be observed with other vibrational transitions. In contrast to this observation, the combined O–H/O···O overtone appears to be of a very high intensity in the Zundel cation (H<sub>5</sub>O<sub>2</sub><sup>+</sup>).<sup>40</sup> We believe that in both cases further comparison to MPANO is not reasonable, since both the transition frequencies of hydrogen bond moieties and their corresponding intensities vary significantly with the strength and geometry of the hydrogen bond, which are reflected in quite diverse potential energy surfaces. Similar conclusions can be drawn from a comparison of the O–H stretching overtone of MPANO with that of the hydrogen maleate ion.<sup>41</sup> In the latter the O–H stretching overtone has a very high intensity in contrast to MPANO where its intensity is moderate. Again, this difference can be attributed to the different shape of the PES in these two systems.

## 5. CONCLUSIONS

In this article we calculated the potential energy surface  $V = V(r_{\text{OH}}, r_{\text{OO}})$  of the strong intramolecular hydrogen-bonded system 4-methoxypicolinic acid *N*-oxide on a medium high DFT level (B3LYP/6-31+G(d,p)). The corresponding dipole moment function was calculated on the same level. We solved the time-independent Schrödinger equation using a rectangular grid basis set and a Gaussian basis set. The vibrational spectrum and metric parameters were calculated, and the effects of deuteration were considered. The band corresponding to asymmetric O–H stretching occurring at about 1400 cm<sup>−1</sup> compares well with the experimental O–H asymmetric stretching band centered at 1380 cm<sup>−1</sup>. We demonstrated that individual vibrational transitions (overtones and hot transitions) of considerable intensities are smeared over a large area and contribute to the broadening of the O–H stretching band. A comparison with the vibrational spectra of some other hydrogen-bonded systems was made. We also show that the basis set consisting of Gaussian basis functions is the method of choice when high accuracy of the eigenvalues is required or when extending the calculations to more dimensions. Moreover we have shown that for large number of basis functions the Gramm-Schmidt orthogonalization procedure outperforms other orthogonalization procedures.

## ACKNOWLEDGMENT

Financial support from the Slovenian Ministry of Higher Education, Science and Technology (grant P1-0012) is gratefully acknowledged. The authors would like to thank Mrs. Charlotte Taft-Krzan for linguistic corrections.

## APPENDIX

**Gramm-Schmidt Orthogonalization.** For the sake of completeness we describe the GS orthogonalization below. GS orthogonalization is based on setting the original basis functions ( $\phi_i$ ) to be orthogonal to all the ones that already have been orthogonalized ( $\chi_i$ ). The first orthogonalized basis function  $\chi_1$  is set to be equal to the original basis function  $\phi_1$ , i.e.  $\chi_1 = \phi_1$ . All the following functions are then orthogonalized using the recursive relation

$$\chi_i = \phi_i + \sum_{j=1}^{i-1} \lambda_{ij} \chi_j \quad (6)$$

where  $\lambda_{ij}$  are the corresponding coefficients. However, it is more reasonable to expand  $\chi_i$  only in terms of the original basis functions, i.e.

$$\chi_i = \sum_{j=1}^i \vartheta_{ij} \phi_j \quad (7)$$

with  $\vartheta_{ij}$  being the corresponding coefficients in the expansion. In each step of the recursion, the coefficients  $\lambda$  and  $\vartheta$  are related in the following way:

$$\begin{aligned} \lambda_{ij} &= - \sum_{l=1}^j \vartheta_{il} S_{il} \\ \vartheta_{ij} &= \sum_{l=1}^{i-1} \lambda_{il} \vartheta_{lj} \end{aligned} \quad (8)$$

$S_{il}$  is the overlap integral of basis functions  $\phi_i$  and  $\phi_l$ , available in the overlap matrix. The initial step of the recursion sets  $\vartheta_{11} = \lambda_{11} = 1$ . At the end of the procedure, the functions are normalized, such that

$$\tilde{\vartheta}_{ij} = \frac{\vartheta_{ij}}{\sqrt{\sum_{j=1}^i \sum_{l=1}^i \vartheta_{ij} \vartheta_{il} S_{il}}} \quad (9)$$

where  $\tilde{\vartheta}_{ij}$  are the normalized coefficients. The resulting matrix consisting of  $\tilde{\vartheta}_{ij}$  is the matrix  $X^\dagger$  required for orthogonalization (eq 3). It features a lower triangular form; hence the multiplication in eq 3 can be greatly simplified in the program code. Both GS and canonical orthogonalization are  $N^3$  procedures, where  $N$  is the number of basis functions. Due to the simpler form of the orthogonalization matrix, the procedure using a GS algorithm is less CPU-intensive (see below).

**Computational Schemes Used.** Vibrational SE in the fitted analytical PES was solved according to the following independent schemes: 1. grid basis set, 2a. Gaussian basis set, symmetric (Löwdin) orthogonalization; 2b. Gaussian basis set, canonical orthogonalization; and 2c. Gaussian basis set, Gramm-Schmidt orthogonalization.

A Gaussian basis function has the functional form

$$\phi_i(x, y) = N_i e^{-\alpha_i(x-x_i^0)^2} e^{-\beta_i(y-y_i^0)^2} \quad (10)$$

As with the analytical expression of the PES,  $N_i$  is the normalization factor,  $x_i^0$  and  $y_i^0$  are the location of the center, and  $\alpha_i$  and  $\beta_i$  are the exponential factors of the  $i$ th Gaussian basis function  $\phi_i$ . For our model system, the basis set parameters, such as the number of basis functions and exponential factors, were optimized to yield reliable results while keeping CPU use as low as possible.

**Computational Performance.** Table 6 lists the minimal basis set sizes for the above schemes that still yields converged results (the criterion for “reliable results” was energy matching within 1 cm<sup>−1</sup> for the 10 lowest levels and



**Table 6.** Minimal Number of Basis Set Functions ( $N_{b_x}$ ,  $N_{b_y}$  and  $N_b = N_{b_x} \times N_{b_y}$ ) Required for Reliable Solutions of the Vibrational Schrödinger Equation for 4-Methoxypicolinic Acid N-Oxide According to the Schemes<sup>a</sup>

scheme	$N_{b_x}$	$N_{b_y}$	$N_b$
1	22	30	660
2a, 2b, 2c	15	26	390

<sup>a</sup> Schemes: 1 - grid basis set; 2a - Gaussian basis set, symmetric orthogonalization; 2b - Gaussian basis set, canonical orthogonalization; and 2c - Gaussian basis set, Gramm-Schmidt orthogonalization.

**Table 7.** CPU Times (in s) for Various Computational Schemes (See Text), Basis Set Sizes, and Routines of the Program<sup>a</sup>

20 × 20 basis set harmonic oscillator				
	O	H'	D	Σ
1	—	—	2.2	2.2
2a	5.8	2.9	4.2	12.9
2b	2.0	2.9	4.1	9.0
2c	1.3	1.4	2.9	5.6
30 × 30 basis set harmonic oscillator				
	O	H'	D	Σ
1	—	—	27.4	27.4
2a	77.1	34.1	52.8	164.0
2b	27.4	33.0	53.7	114.1
2c	27.4	23.2	37.2	87.8
40 × 40 basis set harmonic oscillator				
	O	H'	D	Σ
1	—	—	175.0	175.0
2a	453.3	265.6	347.1	1066.0
2b	155.7	201.9	290.6	648.2
2c	213.8	100.1	207.8	521.7
20 × 20 basis set harmonic oscillator				
	O	H'	D	Σ
1	—	—	600.8	600.8
2a	1756.7	882.3	1166.0	3805.0
2b	616.0	798.3	1282.1	2696.4
2c	1195.4	538.2	781.8	2515.4
optimal basis set MPANO				
	O	H'	D	Σ
1 (22 × 30)	—	—	12.4	12.4
2a (15 × 26)	4.8	2.0	3.8	10.6
2b (15 × 26)	2.1	2.6	3.8	8.5
2c (15 × 26)	2.1	1.3	3.0	7.4

<sup>a</sup> O - orthogonalization; H' - calculation of the Hamiltonian matrix in an orthogonal base; D - diagonalization of the Hamiltonian matrix; Σ - total time. Note that the code has been compiled with the g77 Fortran compiler with the "-malign-double -O6 -march=athlon" for the optimal performance. The calculations have been performed on PC-Linux AMD Athlon (32-bit) workstations.

within 5 cm<sup>-1</sup> for the 11th–20th levels, with respect to levels calculated by a very large, e.g., 60 × 60, Gaussian or rectangular basis set). It is clear that a Gaussian basis set requires fewer basis functions than a rectangular basis set, since displaced Gaussian functions generally resemble Gauss-Hermite polynomials that are eigenfunctions of a harmonic oscillator; hence they are better suited to represent vibrational wavefunctions of realistic systems. The applied vibrational basis set was placed on a rectangular grid. The exponential constants for the  $x$  and  $y$  directions were set to  $\alpha = 70 \text{ Å}^{-2}$  and  $\beta = 250 \text{ Å}^{-2}$ .

Efficiency and the performance of the above schemes was initially tested on a simple 2D harmonic oscillator model

using basis sets of several sizes, since analytical values for the eigenvalues are available for this system. The optimal Gaussian basis sets for MPANO, described above, were also tested. Table 7 lists the required CPU times for various subroutines of the program for solving the vibrational SE. It is clear that the grid basis calculation is much faster than any calculation using the Gaussian basis for the same number of basis functions, since orthogonalization is avoided and the potential energy matrix elements are simpler. It should be noted, however, that calculations using a Gaussian basis require considerably fewer basis functions for realistic systems (e.g., 390 versus 660 in the present case); this outbalances the advantage of a grid basis set at least for 2D vibrational problems. Thus, application of the Gaussian basis set can save a lot of computer resources, particularly the amount of required memory, which can easily extend beyond the range available on contemporary computers. It however remains a challenge to apply the advanced diagonalization schemes that provide only a selected number of the lowest eigenvectors and eigenvalues that are typically interesting for the equilibrium vibrational spectroscopy experiments.

Out of the three orthogonalization schemes, the GS scheme is the least CPU-demanding. This is likely due to the simplified matrix multiplication and diagonalization rather than advantages in obtaining the orthogonalization matrix itself; it should be noted that the orthogonalization matrix obtained by the GS scheme features a lower triangular form which makes the performance of matrix multiplication and diagonalization faster.

## REFERENCES AND NOTES

- (1) Warshel, A. *Computer Modelling of Chemical Reactions in Enzymes and Solutions*; John Wiley and Sons: New York, 1991.
- (2) Warshel, A.; Papazyan, A.; Kollman, P. A. On Low-Barrier Hydrogen Bonds and Enzyme Catalysis. *Science* **1994**, 269, 102–104.
- (3) Cleland, W. W.; Kreevoy, M. M. On Low-Barrier Hydrogen Bonds and Enzyme Catalysis. *Science* **1995**, 269, 102–103.
- (4) Garcia-Viloca, M.; Gao, J.; Karplus, M.; Truhlar, D. G. How Enzymes Work: Analysis by Modern Rate Theory and Computer Simulations. *Science* **2004**, 303, 186–195.
- (5) Benkovic, S. J.; Hammes-Schiffer, S. Enzyme motions inside and out. *Science* **2006**, 312, 208–209.
- (6) *Isotope Effects In Chemistry and Biology*; Kohen, A., Limbach, H. H., Eds.; Taylor & Francis: Boca Raton, FL, 2005.
- (7) *Quantum Medicinal Chemistry*; Carloni, P., Alber, F., Eds.; Wiley: Weinheim, 2003.
- (8) Kiefer, P. M.; Hynes, J. T. Free Energy Relationship for Adiabatic Proton Transfer Reactions in a Polar Environment. I. Fixed Proton Donor-Acceptor Separation. *J. Phys. Chem. A* **2002**, 106, 1834–1849.
- (9) Piana, S.; Carloni, P. Conformational flexibility of the catalytic Asp dyad in HIV-1 Protease: An ab initio study of the free enzyme. *Proteins* **2000**, 39, 26–36.
- (10) Olsson, M. H. M.; Mavri, J.; Warshel, A. Transition State Theory can be used in Studies of Enzyme Catalysis; Lessons from Simulation of Tunneling in Lipoygenase and Other Systems. *Philos. Trans. R. Soc. London, Ser. B* **2006**, 361, 1417–1432.
- (11) Brzezinski, B.; Szafran, M. H NMR studies of solvent and substituent effects on strong intramolecular hydrogen bonds. *Org. Magn. Reson.* **1981**, 15, 78–82.
- (12) Stare, J.; Mavri, J.; Ambrožič, G.; Hadži, D. Strong intramolecular hydrogen bonds. Part I. Vibrational frequencies of the OH group in some picolinic acid N-oxides predicted from DFT calculated potentials and located in the infrared spectra. *J. Mol. Struct. (THEOCHEM)* **2000**, 500, 429–440.
- (13) Perrin, C. L.; Nielson, J. B. "Strong" hydrogen bonds in chemistry and biology. *Annu. Rev. Phys. Chem.* **1997**, 48, 511–544.
- (14) Panek, J.; Stare, J.; Hadži, D. From the isolated molecule to oligomers and the crystal: A static density functional theory and Carr-Parrinello molecular dynamics study of geometry and potential function modifications of the short intramolecular hydrogen bond in picolinic acid N-oxide. *J. Phys. Chem. A* **2004**, 108, 7417–7423.

- (15) Bowman, J. M. Self-consistent field energies and wavefunctions for coupled oscillators. *J. Chem. Phys.* **1978**, *68*, 608–610.
- (16) Bowman, J. M. The Self-Consistent-Field Approach to Polyatomic Vibrations. *Acc. Chem. Res.* **1986**, *19*, 202–208.
- (17) Chaban, G.; Jung, J. O.; Gerber, B. Ab Initio Calculation of Anharmonic Vibrational States of Polyatomic Systems: Electronic Structure Combined with Vibrational Self-Consistent Field. *J. Chem. Phys.* **1999**, *111*, 1823–1829.
- (18) Marston, C. C.; Balint-Kurti, G. G. The Fourier grid Hamiltonian method for bound state eigenvalues and eigenfunctions. *J. Chem. Phys.* **1989**, *91*, 3571–3576.
- (19) Webb, S.; Iordanov, T.; Hammes-Schiffer, S. Multiconfigurational nuclear-electronic orbital approach: Incorporation of nuclear quantum effects in electronic structure calculations. *J. Chem. Phys.* **2002**, *117*, 4106–4118.
- (20) Clabo, D. A.; Allen, W. D.; Remington, R. B.; Yamaguchi, Y.; Schaefer, H. F., III. A systematic study on molecular vibrational anharmonicity and vibration-rotation interaction by self-consistent-field higher-derivative methods. Asymmetric top molecules. *Chem. Phys.* **1988**, *123*, 187–239.
- (21) Stare, J.; Mavri, J. Numerical Solving One- and Two-dimensional Vibrational Time Independent Schrödinger Equation by Variational Method. *Comput. Phys. Commun.* **2002**, *143*, 222–240.
- (22) Stare, J.; Balint-Kurti, G. G. Fourier Grid Hamiltonian Method for Solving the Vibrational Schrödinger Equation in Internal Coordinates: Theory and Test Applications. *J. Phys. Chem. A* **2003**, *117*, 7204–7214.
- (23) Szabo, A.; Ostlund, N. S. *Modern Quantum Chemistry*; Macmillan: 1982.
- (24) There are several useful references describing this algorithm, see for example: <http://www.mathworld.wolfram.com/Gram-SchmidtOrthonormalization.html> (accessed month year).
- (25) Mijoule, C.; Allavena, M.; Leclercq, J. M.; Bouteiller, Y. Theoretical vibrational study of the symmetric  $\nu_{OH}$  and  $\nu_{O...O}$  stretching modes of the formic acid dimer in the gas phase. *Chem. Phys.* **1986**, *109*, 207–213.
- (26) Bouteiller, Y.; Latajka, Z. Theoretical interpretation of acetone–HF infrared spectrum in the gas phase. *J. Chem. Phys.* **1992**, *97*, 145–149.
- (27) Vener, M. V.; Kuehn, O.; Sauer, J. The infrared spectrum of the O...H...O fragment of  $H_5O_2^+$ : Ab initio classical molecular dynamics and quantum 4D calculations. *J. Chem. Phys.* **2001**, *114*, 240–249.
- (28) Frisch, M. J.; Trucks, G. W.; Schlegel, H. B.; Scuseria, G. E.; Robb, M. A.; Cheeseman, J. R.; Montgomery, J. A.; Vreven, T.; Kudin, K. N.; Burant, J. C.; Millam, J. M.; Iyengar, S. S.; Tomasi, J.; Barone, V.; Mennucci, B.; Cossi, M.; Scalmani, G.; Rega, N.; Petersson, G. A.; Nakatsuji, H.; Hada, M.; Ehara, M.; Toyota, K.; Fukuda, R.; Hasegawa, J.; Ishida, M.; Nakajima, T.; Honda, Y.; Kitao, O.; Nakai, H.; Klene, M.; Li, X.; Knox, J. E.; Hratchian, H. P.; Cross, J. B.; Adamo, C.; Jaramillo, J.; Gomperts, R.; Stratmann, R. E.; Yazyev, O.; Austin, A. J.; Cammi, R.; Pomelli, C.; Ochterski, J. W.; Ayala, P. Y.; Morokuma, K.; Voth, G. A.; Salvador, P.; Dannenberg, J. J.; Zakrzewski, V. G.; Dapprich, S.; Daniels, A. D.; Strain, M. C.; Farkas, O.; Malick, D. K.; Rabuck, A. D.; Raghavachari, K.; Foresman, J. B.; Ortiz, J. V.; Cui, Q.; Baboul, A. G.; Clifford, S.; Cioslowski, J.; Stefanov, B. B.; Liu, G.; Liashenko, A.; Piskorz, P.; Komaromi, I.; Martin, R. L.; Fox, D. J.; Keith, T.; Al-Laham, M. A.; Peng, C. Y.; Nanayakkara, A.; Challacombe, M.; Gill, P. M. W.; Johnson, B.; Chen, W.; Wong, M. W.; Gonzalez, C.; Pople, J. A. *Gaussian 03, Revision B.03*; Gaussian, Inc.: Pittsburgh, PA, 2003.
- (29) Wilson, E. B.; Decius, J. C.; Cross, P. C. *Molecular vibrations: the theory of infrared and Raman vibrational spectra*; McGraw-Hill: New York, 1955.
- (30) Morrison, C. A.; Siddick, M. M.; Camp, P. J.; Wilson, C. C. Toward Understanding Mobile Proton Behavior from First Principles Calculation: The Short Hydrogen Bond in Crystalline Urea-Phosphoric Acid. *J. Am. Chem. Soc.* **2005**, *127*, 4042–4048.
- (31) Borstnik, B. Model Calculation of Weak and Medium Strong Linear Hydrogen Bonded Systems. *Chem. Phys.* **1976**, *15*, 391–396.
- (32) Hadži, D.; Bratos, S. In *The hydrogen bond theory*; Schuster, P., Zundel, G., Sandorfy, C., Eds.; North Holland: Amsterdam, 1976; p 567.
- (33) Marechal, Y. IR spectra of carboxylic acids in the gas phase: A quantitative reinvestigation. *J. Chem. Phys.* **1987**, *87*, 6344–6353.
- (34) Witkowski, A.; Wojcik, M. Infrared spectra of hydrogen bond a general theoretical model. *Chem. Phys.* **1973**, *1*, 9–16.
- (35) Lill, M. A.; Helms, V. Compact parameter set for fast estimation of proton transfer rates. *J. Chem. Phys.* **2001**, *114*, 1125–1132.
- (36) Billeter, S. R.; Webb, S. P.; Iordanov, T.; Agarwal, P. K.; Hammes-Schiffer, S. Hybrid approach for including electronic and nuclear quantum effects in molecular dynamics simulations of hydrogen transfer reactions in enzymes. *J. Chem. Phys.* **2001**, *114*, 6925–6936.
- (37) Mavri, J.; Grdadolnik, J. Proton Transfer Dynamics in Acetylacetone: A Mixed Quantum-Classical Simulation of Vibrational Spectra. *J. Phys. Chem. A* **2001**, *105*, 2045–2051.
- (38) Del Bene, J. E.; Jordan, M. J. T.; Gill, P. M. W.; Buckingham, A. D. An *ab initio* study of anharmonicity and matrix effects on the hydrogen-bonded  $BrH:NH_3$  complex. *Mol. Phys.* **1997**, *92*, 429–439.
- (39) Bouteiller, Y.; Latajka, Z. Theoretical interpretation of acetone–HF infrared spectrum in the gas phase. *J. Chem. Phys.* **1992**, *97*, 145–149.
- (40) Stoyanov, E. S.; Reed, C. A. IR spectrum of the  $H_5O_2^+$  cation in the context of proton solvates  $L-H^+-L$ . *J. Phys. Chem. A* **2006**, *110*, 12992–13002.
- (41) Ilczyszyn, M. M.; Baran, J.; Ratajczak, H.; Barnes, A. J. Polarized infrared spectra of potassium hydrogen maleate and potassium deuterium maleate single crystals. *J. Mol. Struct.* **1992**, *270*, 499–515.
- (42) Robertson, J. M.; Ubbelohde, A. R. Structure and Thermal Properties Associated with Some Hydrogen Bonds in Crystals. I. The Isotope Effect. *Proc. R. Soc. London, Ser. A* **1939**, *170*, 222–241.

CI600491P